A Caging Strategy for Tuning the Magneto-Optical Properties of Cobalt Ferrite using a Single Plasmonic Nanoparticle

*Martín Testa-Anta,[1,2] Ana Sousa-Castillo,[2] Alberto López-Ortega,[3] Miguel A. Correa-Duarte,[2] Antonio García-Martín,[4] Paolo Vavassori,[5] Verónica Salgueiriño,[1,2]**

[1] Departamento de Física Aplicada, Universidade de Vigo, 36310 Vigo, Spain

[2] CINBIO, Universidade de Vigo, 36310 Vigo, Spain

[3] Instituto de Nanociencia, Nanotecnología y Materiales Moleculares and Dpto. de Física Aplicada, Universidad de Castilla-La Mancha, Campus Fábrica de Armas, 45071 Toledo, Spain

[4] Instituto de Micro y Nanotecnología IMN-CNM, CSIC, CEI UAM+CSIC, Isaac Newton 8, Tres Cantos, Madrid 28760, Madrid, Spain

[5] CIC-Nanogune, 20018 Donostia-San Sebastián and IKERBASQUE, 48013 Bilbao, Spain

KEYWORDS: Magneto-optical activity, Surface plasmon resonance, Faraday effect, Spinel ferrite.

ABSTRACT

The composite nanostructures with magnetic and plasmonic functionalities herein described were produced according to a unique synthetic strategy by which numerous cobalt ferrite nanoparticles accompanied by an individual gold nanoparticle were confined in silica capsules. This assembly offers a distinctive system on which proving the influence of the surface plasmon of a single 20 or 60 nm-in-diameter gold nanoparticle to increase the visible range magneto-optical activity of the cobalt ferrite magnetic material. Consequently, it provides a key strategy for the production of nanostructures including different materials as building blocks, on which taking advantage of the confined coupling for the development of materials with enhanced magneto-optical capabilities.

The collective oscillations of electrons at metal/dielectric interfaces, known as surface plasmons, can become coupled to electromagnetic waves. As these plasmonic modes confine the electromagnetic fields to subwavelength volumes, the local intensity of the fields becomes greatly increased.[1] As a result, this property permits the magnification of the interactions of light with matter and accordingly, it can be used to manipulate the optical response of a dielectric material[2] or the magneto-optical (MO) response of a magnetic material.[3-5] In particular, MO phenomena considering the Faraday (or Kerr) effect are being under study with the aim of controlling the polarization of transmitted (or reflected) light.[6,7] This control of the MO properties of a magnetic material can lead to many optical devices where magnetism is applied, and becomes therefore of special interest for applications in integrated nanophotonics (magnetoplasmonic sensors,[8-10] photonic devices for integrated Faraday isolators and rotators in photonic circuitry[11-14]) or heat-assisted magnetic recording.[15] It also offers a suitable strategy in the field of metamaterials, *via* manipulating both electric permittivity and magnetic permeability.[16]

This interaction of light with matter, in terms of the MO response of the magnetic material, can be pondered according to the rotation of the polarization of the incident light, observed either in transmission (Faraday rotation) or in reflection (Kerr rotation),[17] and for that, it is required the integration of the optical resonances of plasmonic nanostructures in a, or jointly with, a magnetic material. Different advances in this regard have spurred an interest to design and fabricate devices based on magneto-plasmonic effects.[18-23] However, besides the need to develop inexpensive, reproducible and scalable methods for the production of these nanostructures while enhancing and controlling the MO properties, there is an open question about the effect a single plasmonic system exerts onto the magnetic counterpart (or onto other materials, such as semiconductors for

photocatalysis or on molecules, for example for surface-enhanced Raman spectroscopy, SERS), in order to tabulate it and control it, and not yet reported.

Herein, we have designed a unique synthetic strategy by which the development of MO nanostructures is achieved, containing both magnetic and plasmonic functionalities in confined spaces by a controlled assembly. Thus, we take the first experimental step towards answering the fundamental question regarding the influence of an individual plasmonic nanoparticle on the MO response of a magnetic material, in this case the cobalt ferrite.[24-25] To this end, we have measured the modified optical Faraday rotation and ellipticity of cobalt ferrite nanoparticles trapped inside submicron sized silica capsules, employing the plasmon resonance of an also confined single noble metal (Au) nanoparticle of 20 or 60 nm in diameter. This particular arrangement of plasmonic and magnetic functionalities leads to the observation of changes in the MO activity, with a relative increase at frequencies close to the optical resonance of the plasmonic functionality.

Results and Discussion

The composite nanostructures with magnetic and plasmonic functionalities herein described were produced according to a new synthetic strategy by which numerous cobalt ferrite nanoparticles accompanied by just one gold nanoparticle were confined in silica capsules, as schematically shown in Figure 1a (see the experimental section in the supporting information (SI)). The system has been designed in such a way that it allows to study the properties of these MO assemblies isolated, with a 30-nm thick silica shell keeping them at least 60 nm apart. For the production of these capsules, first and independently, gold nanoparticles of 20 (± 3) and 60 (± 5) nm average diameter were synthesized.[26,27] Figure S1 (in the SI) includes TEM images (a, b) and the UV-vis spectra (d, e) of both types of gold nanoparticles employed in this study. These two

types of gold nanoparticles, in independent experiments, were used as seeds to grow polystyrene (PS) spheres (up to an average diameter of 450 (± 10) nm), leading to Au-PS dimers (see scheme in figure 1a, on the left). PS spheres were also grown in the absence of gold nanoparticles to obtain the reference sample. Subsequently, the PS spheres and the Au-PS dimers were used as substrates on which depositing cobalt ferrite nanoparticles of 16 (± 6) nm average diameter.[28] Figures S1c and S1f (in the SI) include a representative TEM image and the room-temperature field-dependent magnetization of these magnetic nanoparticles, respectively. For this deposition, the layer-by-layer (LbL) self-assembly technique, taking advantage of two layers of polyelectrolytes, permits to attain a homogeneous distribution of the magnetic nanoparticles onto the PS spheres or the Au-PS dimers surface, as becoming adsorbed by electrostatic interactions.[29] Upon the cobalt ferrite deposition, the composite nanostructures were additionally coated with a silica shell (30 (± 4) nm thick) using the Stöber method conditions.[30] Finally, a calcination step (in air and at 600 °C) to remove the PS template, the residual polyelectrolytes and the nanoparticle capping agents, that induces as well some changes in the crystalline structure of the spinel ferrite, was carried out. Consequently, hollow silica capsules containing multiple cobalt ferrite nanoparticles (sample C-Ref), or containing multiple cobalt ferrite nanoparticles and one single gold nanoparticle of 20 or 60 nm (hereafter labelled as samples C-Au20 and C-Au60, respectively) were produced. Figures S2 and S3 (in the SI) include TEM images showing these intermediate steps described.

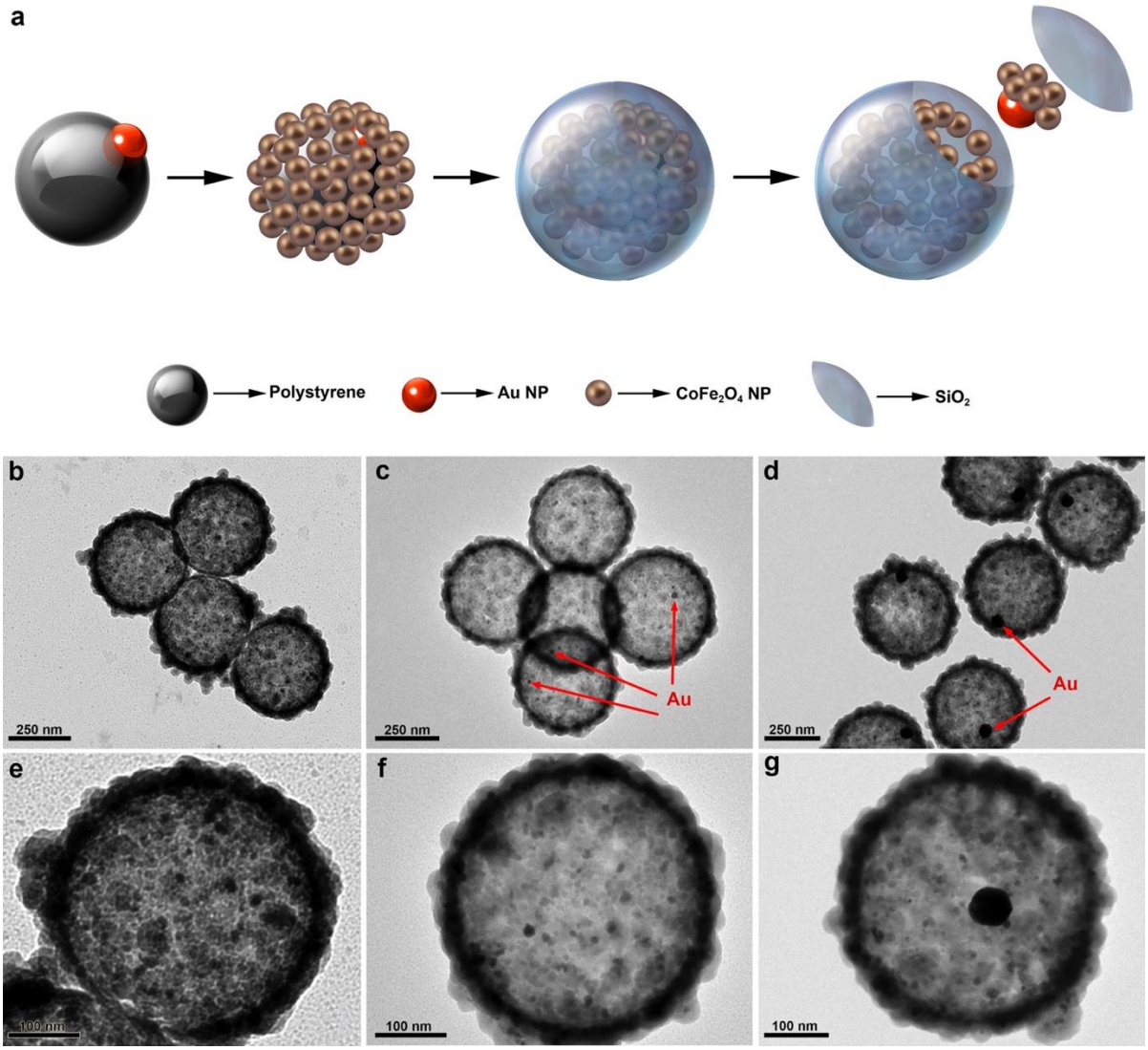

Figure 1. Scheme with the different steps of the synthetic process employed for the production of silica capsules with magnetic and plasmonic functionalities (a), and representative TEM images of the three different types of capsules synthesized at lower and higher magnification: C-Ref (b, e), C-Au20 (c, f) and C-Au60 (d, g). Red arrows indicate the position of the single gold nanoparticle included in every capsule.

The two types of magneto-plasmonic silica capsules have a 510 (± 10) nm average diameter and include one gold nanoparticle of either 20 (± 3) nm or 60 (± 5) nm in diameter and *ca* <1500

nanoparticles of cobalt ferrite per capsule. This estimated value of magnetic nanoparticles inside every capsule was calculated considering half the theoretical value of identical hard spheres (16 nm in diameter) onto the equivalent flat surface of a 450 nm polystyrene sphere, assuming a hexagonally close packing and taking the curved surface into account.[31,32] The additional reference sample consisting of multiple cobalt ferrite nanoparticles trapped inside the silica capsules, but without gold, has a rather similar average diameter (505 (± 8) nm). Figures 1b, 1c and 1d include representative TEM images displaying an overview of the three samples synthesized, on which we can appreciate the homogeneous size of the spherical capsules, the homogeneous silica shell thickness and the uniform distribution of the cobalt ferrite nanoparticles onto the inner surface of the capsules (see also figures S2 and S3 in the SI). The presence of one single metallic nanoparticle in every capsule from samples C-Au20 and C-Au60 is indicated by red arrows (to guide the eye, in figures 1c and 1d). Additionally, figures 1e, 1f and 1g include higher magnification TEM images of capsules from samples C-Ref, C-Au20 and C-Au60, respectively.

The extinction spectra of the three different types of capsules synthesized are shown in Figure 2a. Whereas the surface plasmon resonance peak stemming from each 60 nm gold nanoparticle trapped in every silica capsule can be clearly appreciated at ~546 nm (red spectrum), the one from the 20 nm gold nanoparticles in the C-Au20 sample (blue spectrum) appears entirely screened by the scattering of the cobalt ferrite nanoparticles and the silica shell. This scattering influences the measured absorption as being registered as absorbed light by the instrument, increasing therefore the baseline of the spectrum. Thus, while in the case of the C-Au60 sample, it just screens partially the surface plasmon band, in the case of the C-Au20 sample, this increase in the baseline of the spectrum is sufficient to shade totally the 20-nm gold nanoparticle surface plasmon band. The extinction spectrum of the C-Ref sample just shows the characteristic scattering of cobalt ferrite

nanoparticles inside the silica capsules, with no absorption features in the visible range. Figure 2b includes the field-dependent magnetization of the C-Au20 and the C-Au60 samples, at 300 K and at low fields, stemming solely from the cobalt ferrite (*i.e.* after subtracting the diamagnetic contribution from the gold and silica components) and normalized using the values of saturation magnetization, so that we can appreciate the similar magnetic behavior in both magneto-plasmonic samples.

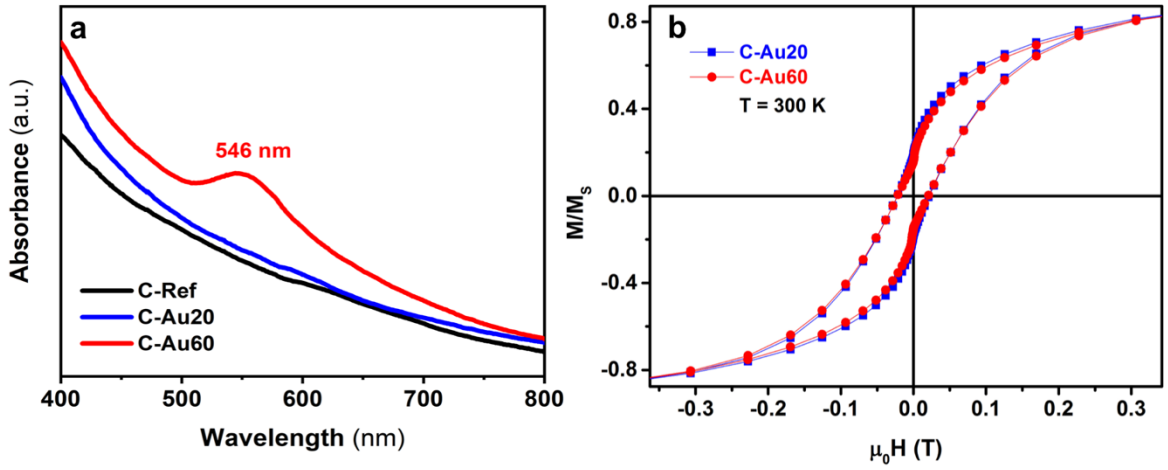

Figure 2. Extinction spectra of the three types of silica capsules synthesized: C-Ref (black), C-Au20 (blue) and C-Au60 (red) (a), and normalized field dependent-magnetization of the C-Au20 and C-Au60 samples at low fields, after subtracting the gold and silica diamagnetic contributions (b).

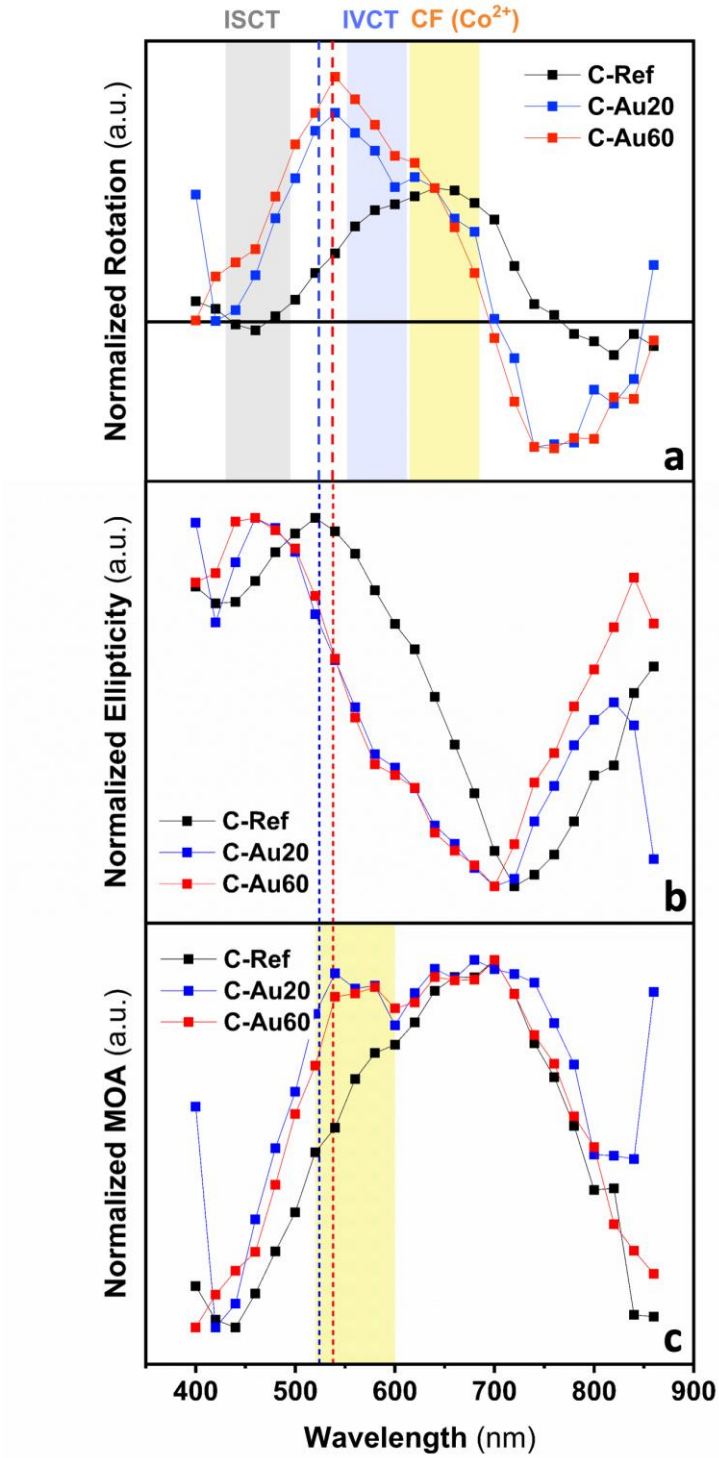

Figure 3. Normalized Faraday rotation (a) and ellipticity (b) spectra of the three types of capsules: C-Ref (in black), C-Au20 (in blue) and C-Au60 (in red), recorded in the visible-near infrared spectral range applying a 0.7 T magnetic field. Magneto-optical activity (MOA) for the three

different types of capsules (c). Vertical dotted blue and red lines indicate the position of the maximum of the localized surface plasmon resonance of the 20 and 60 nm gold nanoparticles in aqueous solution. Pale grey, blue and yellow areas in the Faraday rotation plot indicate the theoretical position of the ISCT, IVCT and CF transitions of the cobalt ferrite and the pale yellow area in the MOA graph frames the range where it becomes enhanced.

Faraday rotation and ellipticity spectra of the three types of capsules were recorded in the visible-near infrared spectral range, while applying a magnetic field of 0.7 T, from which the magneto-optical activity (MOA) spectrum was obtained. For these measurements, the capsules dispersed in water were drop-casted onto glass substrates. Since the intensity of the MOA spectrum is directly related to the concentration of capsules, the impossibility to exert control on this parameter makes it necessary to restrict the evaluation of the results to the line-shape of normalized spectra. Figure 3 includes the normalized spectra of Faraday rotation and ellipticity and of the corresponding MOA for the three types of capsules: C-Ref (in black), C-Au20 (in blue) and C-Au60 (in red). The raw spectra of these three quantities are plotted in Figure S4 (in the SI), as well as the description of their calculation.[33]

Figure 3a includes the normalized Faraday rotation spectra of the three samples. Attending first to the C-Ref sample spectrum, the Faraday rotation shows a maximum located at 650 nm (together with a small shoulder at 580 nm), besides a minimum of rotation at 460 nm. These features are indicative of *d-d* crystal-field (CF) and charge-transfer (CT) transitions within the cobalt ferrite ($CoFe_2O_4$) with a spinel structure, in which an electron through optical excitation is promoted to an excited state within the same ion (on the basis of crystal field splitting) or transferred from one to another neighboring cation, respectively.[24,25,34,35] Two types of CT transitions are typically distinguished: the ISCT (intersublattice charge-transfer), which involves a transition between two

cations located at sites with different crystal symmetry, and the IVCT (intervalence charge-transfer), involving transitions between two cations located at equivalent (or very similar) crystallographic sites.[24,25,36-38] The common feature for inverse spinel ferrites of the $M_xFe_{3-x}O_4$ general type, being M^{2+} a non-magnetic ion, is therefore a set of ISCT transitions between the Fe^{3+} cations lying at the tetrahedral and octahedral sites, denoted by (Fe^{3+}) and [Fe^{3+}], respectively. However, for the inverse cobalt ferrite, where M^{2+} constitutes a magnetic ion, a CF transition because of some tetrahedrally coordinated Co^{2+} ions and an IVCT transition between the Co^{2+} and Fe^{3+} ions located at the octahedral sites can also occur. The transitions observed at 650, 580 and 460 nm for the C-Ref sample are in good agreement with values reported and can be assigned to the $^4A_2$ (^4F) → $^4T_1$(^4P) CF (Co^{2+}), [Co^{2+}]t_{2g} → [Fe^{3+}]t_{2g} IVCT and (Fe^{3+})t_2 → [Fe^{3+}]t_{2g} ISCT transitions in cobalt ferrite, respectively (indicated with shadowed yellow, blue and grey areas in figure 3a). Besides the transitions, the Faraday rotation spectrum, displays values of rotation close to zero in the region at 440-470 nm and a sign crossover to negative rotations occurring at ~770 nm.

The influence of the individual plasmonic nanoparticle in the MO response of the cobalt ferrite nanoparticles trapped in the capsules can therefore be addressed considering the results from the C-Au20 and C-Au60 samples. The resultant spectra (in blue and red, respectively) indicate that the presence of gold blue-shifts the main $CoFe_2O_4$ *d-d* transitions, as well as the Faraday rotation zero-crossing points and most importantly, they show this Faraday rotation becomes increased in the visible range close to the optical resonance of the plasmonic functionality. Similar effects in terms of blue-shifts were observed when considering the Faraday ellipticity measurements (figure 3b and figure S4b, in the SI) of the capsules including the plasmonic gold.

On the basis of the previous results, the MOA spectra for the different types of capsules can be readily calculated and normalized (as shown in figure 3c, the spectra calculated from the raw data are shown in figure S4c, in the SI). The maximum value of MOA reached in the 660-700 nm range for the C-Ref sample (black spectrum), is also displayed in the spectra of the C-Au20 and C-Au60 samples but slightly broadened. Conversely, the samples C-Au20 and C-Au60 display an additional well-defined peak at ~550 nm, both in the Faraday rotation and MOA spectra, which becomes one of the most prominent features. This peak occurs precisely at frequencies close to that of the localized surface plasmon resonance of the gold nanoparticles shown in the UV-vis spectra, that is, at 524 nm and at 538 nm (see the vertical dotted blue and red lines in the graphs in figure 3 to guide the eye). Hence, the Faraday rotation and MOA peaks registered at ~550 nm point to a surface plasmon resonance-induced enhancement effect of the MO response of the cobalt ferrite in the C-Au20 and C-Au60 capsules, on which the gold nanoparticle size (or in terms of the vol.% of Au) should have a crucial role in the MO responses registered. Nevertheless, while the MO spectra were registered at several discrete wavelengths in the 400-860 nm spectral range (with a step of 20 nm), the difference between the plasmon resonance of the 20 and 60 nm Au particles (524 and 538 nm respectively) is actually smaller than this step, and therefore, such a small change in the plasmon resonance cannot be fully ascertained in the MO spectra. Another aspect to point out is the fact that every cobalt ferrite nanoparticle has a different disposition with respect to the plasmonic source, which also means that their MOA become influenced differently, showing the MOA spectra an average effect.

Aiming to shed light on these observations and discard alternative effects, Faraday rotation and ellipticity spectra were also recorded independently for the purely plasmonic nanoparticles, that is, 20 nm (Au20) and 60 nm-sized (Au60) gold nanoparticles (see figure S5 in the SI), and for the

purely magnetic $CoFe_2O_4$ nanoparticles (see figure S6 in the SI). Since no magnetic aggregation is expected for the metallic nanoparticles, the MO measurements were registered in aqueous solution using a 1-mm pathlength cuvette, and the MO signal from the cuvette filled with water was used as reference (referred to as Glass-Water). The observed Faraday rotation for the Au20 and Au60 samples (figures S5a and S5b in the SI) can be mainly associated to the cuvette. However, the ellipticity spectra (figures S5c and S5d in the SI) show distinctive features for these two samples. Both display a change of curvature at the maximum absorption of the localized surface plasmon resonance of the gold nanoparticles, that is, at 524 nm and at 538 nm for the aqueous dispersion of the 20-nm and 60-nm particles, respectively (dotted blue and red lines included in the graph to guide the eye). Anyhow, the negligible Faraday rotation and the small values of Faraday ellipticity (which are two orders of magnitude smaller than those of the C-Ref capsules, see Figure S4, in the SI) of the gold nanoparticles in solution, rule out the possibility of a simple additive effect between the MO response of the magnetic and plasmonic functionalities when considering the Faraday rotation and ellipticity of the capsules from the C-Au20 and C-Au60 samples.

Furthermore, during the synthesis of the capsules, the calcination step to remove the PS and the residual polyelectrolytes and ligands can induce a cation redistribution within the $CoFe_2O_4$ crystalline structure that may lead to differences in the MO spectra. To check this possibility, figure S6 (in the SI) includes the normalized Faraday rotation (a) and ellipticity spectra (b) of the as-synthesized cobalt ferrite nanoparticles ($CoFe_2O_4$, in brown color) and of the capsules reference sample (C-ref, in black color). We can observe that, because of the annealing temperature, the nanoparticles of the magnetic material in the C-ref sample display notable changes in the Faraday rotation and ellipticity curves. These differences can be associated to changes in the Co^{2+}(Td) CF

transition accompanied by a change in the Co^{2+}-Fe^{3+} IVCT transition on octahedral sites,[39] because of the redistribution of the cations or due to an increase of Co^{3+} cations in the spinel structure.[34] These changes stemming from the thermal evolution can be studied by Raman spectroscopy,[39,40] but because of the large scattering of the silica shell in the C-Au20 and C-Au60 samples, we have proceeded by recording the Raman spectra of just cobalt ferrite nanoparticles, as synthesized and after a process of calcination analogous to the one used for the capsules. Figure S7 (in the SI) includes this Raman study and a detailed description, proving the cation redistribution in the spinel crystalline structure and justifying the changes in the rotation and ellipticity registered for the cobalt ferrite nanoparticles calcined inside the capsules. Nonetheless, bearing in mind that the three samples of capsules have undergone the same thermal treatment, similar changes have therefore taken place in both C-Au20 and C-Au60 samples as well as in the C-Ref sample and cannot explain the differences observed in the MOA of the capsules containing the individual plasmonic nanoparticle. The changes observed in the MOA of the cobalt ferrite stem therefore from the plasmon resonance influence of the single gold nanoparticle.

Conclusion

Summarizing, these investigations of the Faraday effect in this particular type of capsules show a plasmon-induced manipulation of the incident light, stemming from one plasmonic nanoparticle, which modifies the polarization of the transmitted light and shifts the sign reversal of the magnetooptical Faraday rotation and ellipticity. Since the magneto-optical activity originates from the spin-orbit coupling and is an intrinsic property of the cobalt ferrite, these results point to the plasmonic effect of the individual metal nanoparticle to increase the magneto-optical activity of the cobalt ferrite in the visible range. Still, it would be interesting to differentiate this influence of

the gold nanoparticle onto the different magnetic ones, a few in close contact and many others gradually far apart from the plasmonic source. Another issue to explore relates to the size of the capsule (with ~ 450 nm internal diameter and therefore close to the surface plasmon resonances), that may create internal resonances as well, modifying the electric field inside and altering the magneto-optics. Anyhow, this confined magneto-plasmonic system opens the door to new pathways for fine tuning the magneto-optics of magnetic nanomaterials. Thus, this work provides a useful caging approach for creating magneto-optical materials stemming from assemblies composed of both plasmonic and magnetic materials on which the plasmonic influence can start from an individual metallic nanoparticle.

ASSOCIATED CONTENT

Supporting Information. The supporting information file includes: the experimental section, figures S1-S7 and the description of the Raman spectroscopy results.

AUTHOR INFORMATION

Corresponding Author

*Verónica Salgueiriño (Email: vsalgue@uvigo.es)

Author Contributions

The manuscript was written through contributions of all authors. All authors have given approval to the final version of the manuscript.

ACKNOWLEDGMENT

The authors acknowledge the financial support from the Xunta de Galicia (Regional Government, Spain) under project ED431C 2016-034 and the Spanish Ministerio de Economía y Competitividad under project CTM2017-84050-R. M. T.-A. acknowledges financial support from the Xunta de Galicia (Regional Government, Spain) under grant 2017-ED481A/322.

REFERENCES

1. Liz-Marzán, L. M. Tailoring Surface Plasmons through the Morphology and Assembly of Metal Nanoparticles. *Langmuir* **2006**, *22*, 32-41.

2. Baron; A., Aradian; A., Ponsinet; V., Barois; P. Self-assembled Optical Metamaterials. *Optics & Laser Tech.* **2016**, *82*, 94-100.

3. Armelles; G., Cebollada; A. García-Martín; A., González; M. U. Magnetoplasmonics: Combining Magnetic and Plasmonic Functionalities. *Adv. Opt. Mater.* **2013**, *1*, 10-35.

4. Bossini; D., Belotelov; V. I., Zvezdin; A. K., Kalish; A. N., Kimel; A. V. Magnetoplasmonics and Femtosecond Optomagnetism at the Nanoscale. *ACS Photonics* **2016**, *3*, 1385-1400.

5. Belotelov; V. I., Akimov; I. A., Pohl; M., Kotov; V. A., Kasture; S., Vengurlekar; A. S., Gopal; A. V., Yakovlev; D. R., Zvezdin; A. K., Bayer; M. Enhanced Magneto-Optical Effects in Magnetoplasmonics Crystals. *Nature Nanotech.* **2011**, *6*, 370-376.

6. Zvezdin; A., Kotov; V. *Modern Magnetooptics and Magnetooptical Materials* (IOP, Bristol and Philadelphia), **1997**.

7. Levy; M., Baryshev; A. V., Inoue; M. (eds). *Magnetophotonics: From theory to applications* (Springer, Berlin, Heidelberg), **2013**.

8. Maccaferri; N., Gregorczyk; K. E., de Thales; V. A. G., Oliveira; M., van Kataja; S., Kijken; Z., Pirzadeh; A., Dmitriev; J., Knez Akerman; M., Vavassori P. Ultrasensitive and Label-free Molecular-level Detection Enabled by Light Phase Control in Magnetoplasmonic Nanoantennas. *Nature Comm.* **2015**, *6*, 6150.

9. Caballero; B., García-Martín; A., Cuevas; J. C. Hybrid Magnetoplasmonic Crystals Boost the Performance of Nanohole Arrays as Plasmonic Sensors. *ACS Photonics* **2016**, *3*, 203-208.

10. Qin; J., Zhang; Y., Liang; X., Liu; C., Wang; C., Kang; T., Lu; L., Zhang; H., Zhou; P., Wang; X., Peng; B., Hu; J., Deng; L., Bi; L. Ultrahigh Figure-of-Merit in Metal-Insulator-Metal Magnetoplasmonic Sensors using Low Loss Magneto-optical Oxide Thin Films. *ACS Photonics* **2017**, *4*, 1403-1412.

11. Floess; D., Hentschel; M., Weiss; T., Habermeier; H.-U., Jiao; J., Tikhodeev; S. G., Giessen; H. Plasmonic Analog of Electromagnetically Induced Absorption leads to Giant Thin Film Faraday Rotation of 14°. *Phys. Rev. X* **2017**, *7*, 021048.

12. Liu; M., Zhang; X. Plasmon-boosted Magneto-Optics. *Nature Photonics* **2013**, *7*, 429-430.

13. Koenderink; A. F., Alú; A. Polman; A. Nanophotonics: Shrinking Light-based Technology. *Science* **2015**, *348*, 516-521.

14. Firby; C. J., Chang; P., Helmy; A. S., Elezzabi; A. Y. Magneoplasmonic Faraday Rotators: Enabling Gigahertz Active Polarization Control for Integrated Plasmonics. *ACS Photonics* **2016**, *3*, 2344-2352.

15. Challener; W. A., Peng; C., Itagi; A. V., Karns; D., Peng; W., Peng; Y.; Yang; X., Zhu; X., Gokemeijer; N. J., Hsia; Y.-T., Ju; G., Rottmayer; R. E., Seigler; M. A., Gage; E. C. Heat-assisted Magnetic Recording by a Near-field Transducer with Efficient Optical Energy Transfer. *Nature Photonics* **2009**, *3*, 220-224.

16. Watts; C. M., Liu; X., Padilla; W. J. Metamaterial Electromagnetic Wave Absorbers. *Adv. Optical Mater.* **2012**, *24*, OP98-120.

17. Scott; G. B., Lacklison; D. E., Ralph; H. I., Page; J. L. Magnetic Circular Dichroism and Faraday Rotation Spectra of $Y_3Fe_5O_{12}$. *Phys. Rev. B* **1975**, *12*, 2562-2571.

18. Li; Y., Zhang; Q., Nurmikko; A. V., Sun; S. Enhanced Magnetooptical Response in Dumbbell-like Ag-$CoFe_2O_4$ Nanoparticle Pairs. *Nano Letters* **2005**, *5*, 1689-1692.

19. Jain; P. K., Xiao; Y., Walsworth; R., Cohen; A. E. Surface Plasmon Resonance Enhanced Magneto-Optics (SuPREMO): Faraday Rotation Enhancement in Gold-coated Iron Oxide Nanocrystals. *Nano Letters* **2009**, *9*, 1644-1650.

20. Wang; L., Clavero; C., Huba; Z., Carroll; K. J., Carpenter; E. E., Gu; D., Lukaszew; R. A. Plasmonics and Enhanced Magneto-Optics in Core-Shell Co-Ag Nanoparticles. *Nano Letters* **2011**, *11*, 1237-1240.

21. López-Ortega; A., Takahashi; M., Maenosono; S., Vavassori; P. Plasmon induced Magneto-Optical Enhancement in Metallic Ag/FeCo Core/Shell Nanoparticles synthesized by Colloidal Chemistry. *Nanoscale* **2018**, *10*, 18672-18679.

22. Fan; B., Nasier; M. E., Nicholls; L. H., Zavats; A. V., Podolsky; V. A. Magneto-Optical Metamaterials: Nonreciprocal Transmission and Faraday Effect Enhancement. *Adv. Optical Mater.* **2019**, *7*, 1801420.

23. Campo; G., Pineider; F., Fantechi; E., Innocenti; C., Caneschi; A., De Julián Fernández; C. Addressing the Influence of Localized Plasmon Resonance on the Magneto-Optical Properties of Cobalt Ferrite Nanoparticles. *J. Nanosci. Nanotech.* **2019**, *19*, 4946-4953.

24. Fontijn; W. F. J., van der Zaag; P. J., Feiner; L. F., Metselaar; R., Devillers; M. A. C. A Consistent Interpretation of the Magneto-optical Spectra of Spinel Type Ferrites. *J. Appl. Phys.* **1999**, *85*, 5100-5105.

25. Kim; K. J., Lee; H. S., Lee; M. H., Lee; S. H. Comparative Magneto-Optical Investigation of d-d Charge-Transfer Transitions in Fe_3O_4, $CoFe_2O_4$, and $NiFe_2O_4$. *J. Appl. Phys.* **2002**, *91*, 9974-9977.

26. Turkevich; J., Stevenson; P. L., Hillier; J. A Study of the Nucleation and Growth Processes in the Synthesis of Colloidal Gold. *Faraday Soc.* **1951**, *11*, 55-75.

27. Bastús; N. G., Comenge; J., Puntes; V. Kinetically Controlled Seeded Growth Synthesis of Citrate-Stabilized Gold Nanoparticles of up to 200 nm: Size Focusing versus Ostwald Ripening. *Langmuir* **2011**, *27*, 11098-11105.

28. Wagner; J., Autenrieth; T., Hempelmann; R. Core Shell Particles consisting of Cobalt Ferrite and Silica as Model Ferrofluids [$CoFe_2O_4$-SiO_2 core shell particles]. *J. Magn. Magn. Mater.* **2002**, *252*, 4-6.

29. Donath; E., Sukhorukow; G. B., Caruso; F., Davis; S. A., Möhwald; H. Novel Hollow Polymer Shells by Colloid-Templated Assembly of Polyelectrolytes. *Angew. Chem. Int. Ed.*, **1998**, *37*, 2201-2205.

30. Stöber; W., Fink; A., Bohn; E. Controlled Growth of Monodisperse Silica Spheres in the Micron Size Range. *J. Coll. Interf. Sci.* **1968**, *26*, 62-69.

31. Grason; G. M. Perspective: Geometrically Frustrated Assemblies. *J. Chem. Phys.* **2016**, *145*, 110901.

32. Testa-Anta; M., Correa-Duarte; M. A., Salgueiriño; V. Self-Assembly of Spherical or Rod-shaped Magnetic Nanocrystals onto Curved Substrates governed by the Radius of Curvature. *Particle & Part. Charact. Syst.* **2018**, 1800046.

33. Vavassori; P. Polarization Modulation Technique for Magneto-Optical Quantitave Vector Magnetometry. *Appl. Phys. Lett*. **2000**, *77*, 1605-1607.

34. Martens; J. W. D., Peeters; W. L., van Noort; H. M., Erman; M. Optical, Magneto-Optical and Mössbauer Spectroscopy on Co^{3+} substituted Cobalt Ferrite $Co^{2+}Fe_{2-x}Co^{3+}{}_xO_4$ ($0 \leq x \leq 2$). *J. Phys. Chem. Solids* **1985**, *46*, 411-416.

35. Tirosh; E., Shemer; G., Markovich; G. Optimizing Cobalt Ferrite Nanocrystal Synthesis using a Magneto-Optical Probe. *Chem. Mater.* **2006**, *18*, 465-470.

36. Feil; H. Intervalence Charge Transfer Transitions in Superconductors and related Compounds. *Solid State Commun.* **1989**, *69*, 245-248.

37. Veis; M., Antos; R., Visnovsky; S., Kulkarni; P. D., Venkataramani; N., Prasad; S., Mistrik; J., Krishnan; R. Complete Permittivity Tensor in Sputtered $CuFe_2O_4$ Thin Films at Photon Energies between 2 and 5 eV. *Materials* **2013**, *6*, 4096-4108.

38. Chen; J., Hsu; H.-S., Huang; Y.-H., Huang; D.-J. Spin-dependent Optical Charge Transfer in Magnetite from Transmitting Optical Magnetic Circular Dichroism. *Phys. Rev. B* **2018**, *98*, 085141.

39. Testa-Anta; M., Rivas-Murias; B., Salgueiriño; V. Spin Frustration drives Exchange Bias Sign Crossover in $CoFe_2O_4$-Cr_2O_3 Nanocomposites. *Adv. Func. Mater.* **2019**, 1900030.

40. Rivas-Murias; B., Salgueiriño; V. Thermodynamic CoO-Co_3O_4 Crossover using Raman Spectroscopy in Magnetic Octahedron-shaped Nanocrystals. *J. Raman Spectroscopy* **2017**, *48*, 837-841.

TOC